Environmental Science & Technology

pubs.acs.org/est

Article

Source Quantification of South Asian Black Carbon Aerosols with Isotopes and Modeling

Sanjeev Dasari, August Andersson, Andreas Stohl, Nikolaos Evangeliou, Srinivas Bikkina, Henry Holmstrand, Krishnakant Budhavant, Abdus Salam, and Örjan Gustafsson*

Cite This: *Environ. Sci. Technol.* 2020, 54, 11771−11779

Read Online

ACCESS | Metrics & More | Article Recommendations | Supporting Information

ABSTRACT: Black carbon (BC) aerosols perturb climate and impoverish air quality/human health—affecting ∼1.5 billion people in South Asia. However, the lack of source-diagnostic observations of BC is hindering the evaluation of uncertain bottom-up emission inventories (EIs) and thereby also models/policies. Here, we present dual-isotope-based ($\Delta^{14}C/\delta^{13}C$) fingerprinting of wintertime BC at two receptor sites of the continental outflow. Our results show a remarkable similarity in contributions of biomass and fossil combustion, both from the site capturing the highly populated highly polluted Indo-Gangetic Plain footprint (IGP; $\Delta^{14}C$-$f_{biomass}$ = 50 ± 3%) and the second site in the N. Indian Ocean representing a wider South Asian footprint (52 ± 6%). Yet, both sites reflect distinct $\delta^{13}C$-fingerprints, indicating a distinguishable contribution of C_4-biomass burning from peninsular India (PI). Tailored-model-predicted season-averaged BC concentrations (700 ± 440 ng m^{-3}) match observations (740 ± 250 ng m^{-3}), however, unveiling a systematically increasing model-observation bias (+19% to −53%) through winter. Inclusion of BC from open burning alone does not reconcile predictions ($f_{biomass}$ = 44 ± 8%) with observations. Direct source-segregated comparison reveals regional offsets in anthropogenic emission fluxes in EIs, overestimated fossil-BC in the IGP, and underestimated biomass-BC in PI, which contributes to the model-observation bias. This ground-truthing pinpoints uncertainties in BC emission sources, which benefit both climate/air-quality modeling and mitigation policies in South Asia.

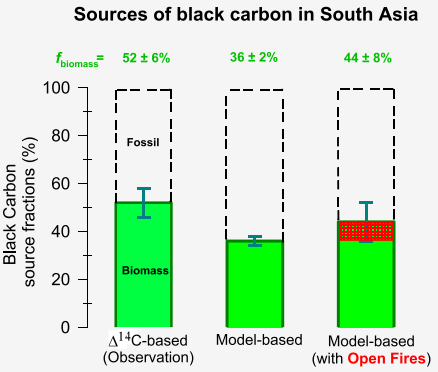

INTRODUCTION

The impacts of combustion-derived black carbon (BC) on regional warming and effects on air quality and human health are large, yet remain highly uncertain, despite considerable recent scientific attention.[1−7] This is particularly troublesome for highly populated, high-pollution regions such as South Asia.[1−3] BC is implicated to also cause a multitude of secondary effects in this region such as monsoon shifts, increased frequencies of storms, surface dimming, melting of glaciers, and disturbance of precipitation patterns affecting both freshwater supply and agriculture.[1,4−6]

Modeling efforts, seeking to constrain the amplitude of perturbations caused by BC, are challenged by several uncertainties.[7] Current atmospheric chemistry-transport and climate models have so far had limited success in mimicking the observed strong seasonal cycle of ground-level BC mass concentrations in South Asia.[8,9] The uncertain contributions from different emission sources (e.g., fossil fuel combustion vs biomass burning) from bottom-up emission inventories (EIs) are likely central to these discrepancies.[8−14] The available EIs provide highly variable BC emission estimates for South Asia ranging from 388 to 1344 Gg/yr[12] (Supporting Information Table S1 and Figure S1). These underlying uncertainties thus need to be reduced as EIs form the basis for modeling of climate and health effects, as well as often serve as the principal input for policy development and mitigation efforts.[2,3,6] Recent assessments advocate for field-based observations of source-diagnostic tracers to evaluate and possibly refine EIs.[3,15]

Top-down observations in the actual atmosphere provide an opportunity to "ground-truth" EI-coupled-model predictions. Despite the high variability in BC emissions from multiple sources, the concentrations in the atmosphere are comparably less variable, reflecting the homogenizing effect of atmospheric mixing. Thus, comparisons with ambient data are crucial to assess and evaluate EIs and atmospheric transport models. Model-observation comparison of concentrations is useful yet provides limited information for evaluating which of the different sources potentially cause concentration offsets.[8,9]

In recent years, the application of dual-carbon isotopes [natural abundance radiocarbon $^{14}C/^{12}C$ (reported as $\Delta^{14}C$) and stable carbon $^{13}C/^{12}C$ (reported as $\delta^{13}C$)] of BC aerosols

Received: April 8, 2020
Revised: September 3, 2020
Accepted: September 4, 2020
Published: September 4, 2020

[here represented by elemental carbon (EC), the mass basis of BC] has proven to be a useful tool to quantitatively constrain the relative contribution from different combustion sources of BC.[16−22] Fossil sources are completely depleted in $\Delta^{14}C$, while biomass sources have a distinct $\Delta^{14}C$ signature that reflects their integrated period of biomass photosynthesis and storage. This allows deconvolution of the relative contributions from combustion of fossil fuel versus biomass (dead-C vs modern-C).[10,13] Furthermore, the $\delta^{13}C$-signature adds specificity for different BC source classes (e.g., coal and liquid fossil, and C_3- and C_4-plants).[16−18] The two-dimensional isotopic signatures of $\Delta^{14}C$ and $\delta^{13}C$ can, therefore, be combined to apportion source contributions to atmospheric BC from different combustion processes.[20−22]

In this paper, we use this dual-carbon isotope approach to fingerprint BC in the S Asian continental outflow intercepted in the Indo-Gangetic Plain (IGP) and over the N. Indian Ocean, respectively. The uncertainties in the dual-isotope endmembers were addressed using a Bayesian statistical framework.[16,17,20−22] The source-segregated observed BC concentrations were then directly compared to tailored predictions of source-segregated BC contributions from an atmospheric transport model, the Flexible Particle Dispersion Model (FLEXPART), coupled to two complementary EIs: Evaluating the Climate and Air Quality Impacts of Short-Lived Pollutants (ECLIPSE) for anthropogenic emissions and the satellite-derived Global Fire Emissions Database (GFED) for open burning emissions.[23−26] Taken together, the comparison between the observation-based (top-down) and FLEXPART-ECLIPSE-GFED (FEG) model-simulated (bottom-up) contributions from different source types allows us to assess the regional-scale variation of sources of BC as well as evaluate the model performance for one of the most polluted regions in the world during the high-loading winter period.

MATERIALS AND METHODS

The South Asian Pollution Experiment 2016 Field Campaign. The high-intensity South Asian Pollution Experiment 2016 (SAPOEX-16) campaign was conducted from 4 January to 24 March 2016.[27] Sampling was carried out at the Bangladesh Climate Observatory at Bhola (BCOB; 22.17°N, 90.71°E; 10 m agl), located on the remote southern end of the Bhola Island, which is on the outflow edge of the IGP, and at the Maldives Climate Observatory at Hanimaadhoo (MCOH; 6.78°N, 73.18°E; 1.5 m agl), located on the northern tip of a northern island in the northernmost atoll of the Republic of the Maldives, south of peninsular India (PI) (i.e., ∼ south of 23.4°N) in the N. Indian Ocean (see Figure 1 for site locations).

Fine size fraction $PM_{2.5}$ aerosol samples (n = 24) were repeatedly collected for 24 h at a time at BCOB, and PM_1 aerosol samples (n = 43) were repeatedly collected for 48 h at MCOH, using identical high-volume samplers (model DH77, Digitel A.G. Switzerland) operated at 500 L/min at both sites (details in Supporting Information Tables S2 and S3). BCOB experienced prolonged power cuts during the February−March period,[28] resulting in a lower number of samples collected during that time.

Measurement of Aerosol Carbon Concentrations. The aerosol organic carbon (OC), EC [here referred to as BC], and total carbon (TC = OC + BC) concentrations were measured with a thermal-optical transmission analyzer (Sunset Laboratory, Tigard, OR, USA) using the National Institute for Occupational Safety and Health (NIOSH) 5040 method. The instrument response was calibrated using potassium hydrogen phthalate, with an overall analytical uncertainty of <3% (1 standard deviation (SD), for n = 5). The instrument analytical precision was ascertained from analysis traceable of The National Institute of Standards and Technology Urban Dust Standard Reference Material 8785 air particulate matter on filter media. Concentration values of OC were also blank corrected by subtracting an average of the field blanks (0.3 ± 0.01 $\mu g\ cm^{-2}$). No BC was detected in the filter blanks. The average relative standard deviation of triplicate analysis was 2.5% at BCOB and 3% at MCOH for TC.

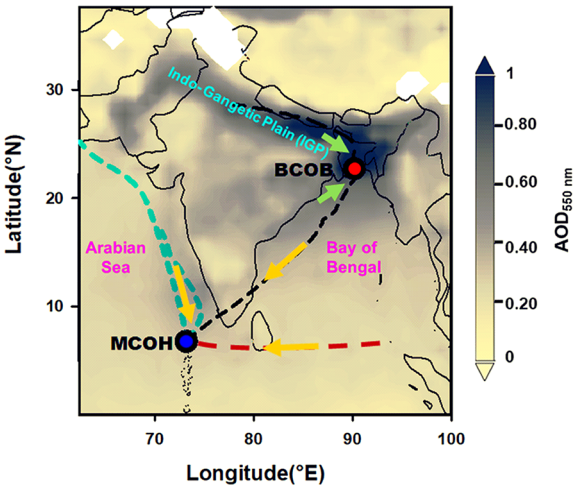

Figure 1. Average AOD at 550 nm from the Moderate Resolution Imaging Spectroradiometer during January-to-March 2016 over the S. Asian region. The receptor sites are shown: the Bangladesh Climate Observatory at Bhola (BCOB, red fill) and the Maldives Climate Observatory at Hanimaadhoo (MCOH, blue fill). The dashed lines show mean air mass back-trajectory clusters, and the arrows represent the air mass transport pathways for the two sites, respectively (see details in Supporting Information Figures S2 and S3).

Carbon Isotope Analysis. To determine the isotopic composition of BC, 9 samples from BCOB and 10 samples from MCOH were chosen for isolation of BC (details in Supporting Information Table S4). These samples have high BC concentrations and are representative of the dominant air mass clusters during the Jan-Feb-Mar period (see Supporting Information Figures S2−S4). The isotopic analysis of BC was performed as described in previous publications.[17−22] Briefly, the CO_2 evolving from the BC phase using the NIOSH 5040 protocol was purified online and cryogenically trapped in glass ampoules for further off-line isotopic analysis. The total sample size was at least 40 μg C. Both carbon isotopes ($\Delta^{14}C$, $\delta^{13}C$) were measured at the United States National Science Foundation National Ocean Science Accelerator Mass Spectrometry facility of Woods Hole Oceanographic Institution (MA).

Although 19 samples were isolated for BC isotopic analysis in total, we are only able to utilize the results of 16 samples (Figure 2). This is because the isolates of two samples (SPX-BHL-114, SPX-MCOH-32) did not contain enough C-amount for $\delta^{13}C$ analysis, and the results of a third sample (SPX-BHL-121) were not used further in discussions and source apportionment calculations (details explained in Supporting Information Table S4; see also Supporting Information Notes S1−S4).

https://dx.doi.org/10.1021/acs.est.0c02193
Environ. Sci. Technol. 2020, 54, 11771−11779

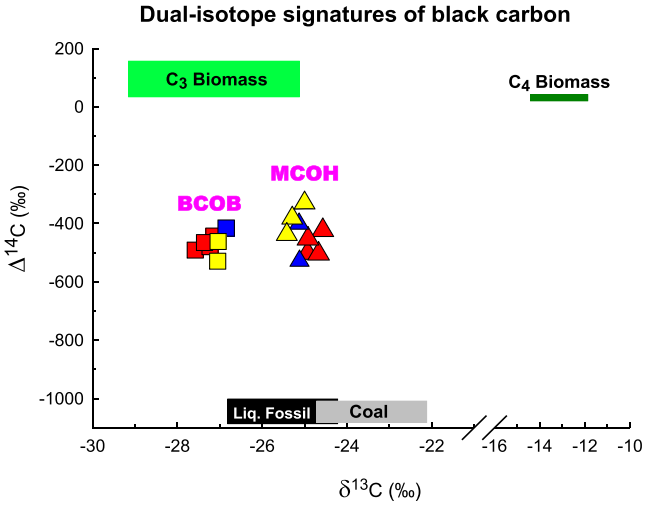

Figure 2. Radiocarbon ($\Delta^{14}C$) and stable isotope ($\delta^{13}C$) signatures of BC during January (red), February (blue), and March (yellow) 2016 are shown for BCOB (squares) and MCOH (triangles). The endmember ranges (Mean ± SD) for C_3 biomass- (light green, top) and C_4 biomass- (dark green, top) burning emissions, liquid fossil fuel combustion (black, bottom), and fossil coal combustion (grey, bottom) are outlined as shaded rectangular bars (endmember constraints are detailed in Supporting Information Table S5; see also Notes S1−S3, respectively).

Estimating Fraction Biomass Burning (f_{bio}) Using Isotopic Mass Balance. The relative contribution to atmospheric BC from biomass burning (f_{bio}; including biofuel and open burning fires) and fossil fuel combustion ($f_{fossil} = 1 - f_{bio}$) sources was calculated with an isotopic mass-balance equation as shown below (see f_{bio} data in Supporting Information Table S4):

$$\Delta^{14}C_{BC} = \Delta^{14}C_{biomass} \times f_{bio} + \Delta^{14}C_{fossil} \times (1 - f_{bio}) \quad (1)$$

Here, $\Delta^{14}C_{BC}$ represents the radiocarbon signature in the ambient samples. $\Delta^{14}C_{fossil}$ is −1000‰, since geologically aged fossil carbon is completely devoid of radiocarbon. Endmember values for contemporary radiocarbon $\Delta^{14}C_{biomass}$ depend on the type and age of the studied biomass, including annual plants, shrubs, and wood.[10,13,17] The $\Delta^{14}C$ of annual plants (fresh biomass) represents the signature of CO_2 for the collection year (+20 ± 10‰ as of 2016, details in Supporting Information Note S1),[29] whereas the signature for wood represents integration of the $\Delta^{14}C$ signature of CO_2 over the growth period of trees, including the decay from the atmospheric ^{14}C injections during the nuclear bomb testing in the early 1960s[29] (+110 ± 70‰ as of 2016; details in Supporting Information Note S1). We here establish a $\Delta^{14}C_{biomass}$ endmember value of +70 ± 35‰, based on existing knowledge on emissions from different major biomass source categories[12] (details in Supporting Information Note S2).

Bayesian Statistical Source Apportionment. In addition to $\Delta^{14}C$, the BC fingerprint may be further refined by also including the $\delta^{13}C$ signature in the analysis.[20−22] For South Asia, there are overall four main source classes with distinct $\delta^{13}C$ values that possibly contribute to the ambient $\delta^{13}C$ signature of BC: C_3-plants (e.g., wood, rice, and wheat), and C_4-plants (e.g., sugarcane and millet), liquid fossil fuel (e.g., traffic), and fossil coal (see Supporting Information Table S5 for isotopic endmember values and also Supporting Information Note S3 for a discussion on fractionation effects).

To resolve the relative source contributions from these different source classes, while accounting for the inherent variability in their endmembers, an isotopic mass balance calculation was used within the framework of a Bayesian Markov chain Monte Carlo (MCMC) scheme.[17,30] This MCMC methodology was developed in detail in a previous publication[17] and has since been implemented in multiple studies.[16,17,20−22] Isotopic signatures of seven samples from BCOB and nine samples from MCOH (Supporting Information Table S4; see also Supporting Information Note S4) were used for conducting SAPOEX-16 BC source apportionment calculations (see Figure 3). By combining

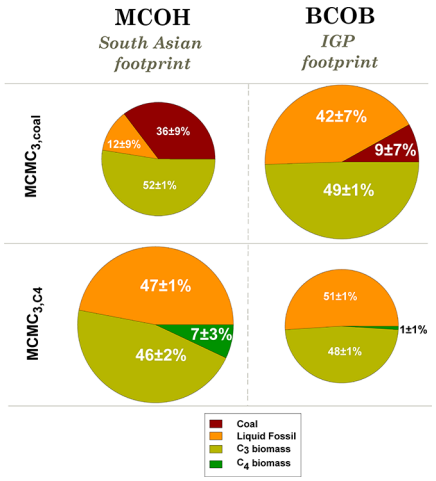

Figure 3. BC source fractions during SAPOEX-16 were computed using MCMC simulations (Mean ± SD) of fossil coal combustion (brown), liquid fossil fuel combustion (orange), and biomass burning C_3-plants (light green) and C_4-plants (dark green). Results from two three-source modeling scenarios ($MCMC_{3,coal}$: C_3 biomass, coal, and liquid fossil fuel and $MCMC_{3,C4}$: C_3 biomass, C_4 biomass, and liquid fossil fuel) are shown (see also Supporting Information Figures S5 and S6). The bigger pie-charts represent the most likely statistical modeling scenario for observed BC isotopic footprints for the IGP (at BCOB; $MCMC_{3,coal}$) and for the wider South Asia (at MCOH; $MCMC_{3,C4}$)

multiple data points, suppression of the influence of endmember variability (e.g., partial overlapping $\delta^{13}C$-signatures of fossil coal and liquid fossil fuel; see Figure 2 and Supporting Information Table S5) on the computed relative source contributions is obtained, following the original method paper.[17] To examine different possible source combination scenarios, three different MCMC computations were carried out for each site (methodological details in Supporting Information Note S5). From these numerical simulations, statistical estimates of the relative source contributions (e.g., mean, standard deviation, and median) are obtained, while the estimated probability density functions are also visualized (Supporting Information Figure S5).

FEG Model. The BC concentrations at MCOH were simulated, for the tailored exact time periods of each of the filter-based collections,[22] using the FEG model[23−26] (see details of model set-up, parameterization, and simulation in Supporting Information Note S6; results in Supporting Information Table S6).

https://dx.doi.org/10.1021/acs.est.0c02193
Environ. Sci. Technol. 2020, 54, 11771−11779

Air Mass Back Trajectories and Identification of Source Regions. For SAPOEX-16, we conducted detailed analysis of air mass back trajectories (Supporting Information Figures S2 and S3). The potential source regions were identified with (i) cluster analysis, (ii) fractional cluster contributions, and (iii) concentrated weighted trajectory (CWT) analysis of BC concentrations (methodological details in Supporting Information Note S7).

RESULTS AND DISCUSSION

Wintertime Aerosol Characteristics and BC Concentrations. Elevated aerosol loadings were observed during SAPOEX-16, reaching an aerosol optical depth (AOD) above 0.4, which is typical for the severe air pollution of wintertime South Asia (Figure 1). Similarly, high aerosol concentrations were recorded at both ground-based observatories MCOH and BCOB (Supporting Information Figure S4). At MCOH, the average concentration of PM_1 in January (31 ± 6 $\mu g\ m^{-3}$) was higher than that in March (19 ± 6 $\mu g\ m^{-3}$). At BCOB, the wintertime average $PM_{2.5}$ levels reached mass concentrations of 104 ± 71 $\mu g\ m^{-3}$, considerably exceeding the WHO ambient air quality standard (25 $\mu g\ m^{-3}$).[3]

Various air mass source regions affected the sampling during SAPOEX-16, allowing a broad air mass classification (Supporting Information Figures S2−S4; see also Supporting Information Note S7). Samples collected during January at both BCOB and MCOH were influenced by air masses from the IGP because of synoptic meteorology.[27] During February and March, samples collected at MCOH were influenced by air masses received from the Arabian Sea (ARS) and South East Asia (SE Asia), respectively. PI (i.e., ∼ south of 23.4°N) was the dominant source region influencing sampling at MCOH in the ARS and SE Asia wind regimes (Feb + Mar) (see Supporting Information Figure S3.d). On the contrary, BCOB received air masses from N Bay of Bengal (N BOB) during both February and March. Although there are fewer samples collected at BCOB ($n = 24$), there are nearly the same number of samples representative of the two different geographical source regions (IGP: $n = 13$; N BOB: $n = 11$; see Supporting Information Figure S4) influencing sampling during winter 2016.

Air mass source regions strongly affected the dynamics of ground-based BC concentrations as well at the two receptor observatories (Supporting Information Figure S4). Overall, at MCOH, BC concentrations in the IGP cluster (871 ± 161 ng m^{-3}) were elevated compared to air from the ARS (640 ± 300 ng m^{-3}) and the SE Asian clusters (608 ± 200 ng m^{-3}). Likewise, at BCOB, where concentrations were about an order of magnitude higher compared to MCOH, BC concentrations in air masses from the IGP (12.3 ± 5.3 $\mu g\ m^{-3}$) were roughly three times larger than in air masses from the N BOB (4.6 ± 3.9 $\mu g\ m^{-3}$). However, the OC/BC ratios for the overlapping time periods were overall similar at MCOH (range: 1.2 to 6.1) and BCOB (range: 1.3 to 4.4), and compared well with previously reported OC/BC values in the region (see detailed comparison in Supporting Information Table S7). Bulk-element markers like the OC/BC ratio are intrinsically nonconservative[13] and thus nonideal for distinguishing quantitatively the relative contribution of BC from fossil versus contemporary biomass combustion sources.

Carbon Isotope-Based Source Apportionment of BC. The $\Delta^{14}C$ data for both BCOB and MCOH are remarkably invariable over the course of the campaign. Using eq 1, the fraction biomass (f_{bio}) was $50 \pm 3\%$ at BCOB, and $52 \pm 6\%$ at MCOH, demonstrating similar contributions from total fossil sources and total biomass sources to the integrated IGP footprint and to the larger South Asian footprint, respectively (Figure 2; see also Supporting Information Table S4). These values are broadly in agreement with previous reports, based on much fewer observations, for wintertime MCOH.[13,18,19] However, here, we present a first direct comparison with the IGP-outflow integrating BCOB. These observational constraints give a different picture compared to estimates from earlier regional modeling and satellite-based inversion studies, which instead have suggested a dominant contribution from biomass burning (including biofuel) to BC, especially over the IGP.[8,9,14] In contrast to reports for other polluted regions such as in East Asia, where the $\Delta^{14}C$-constrained f_{bio} is typically 20−30%,[20] the biomass contributions over South Asia are significantly higher.[13,19,31] Although the powerful $\Delta^{14}C$ signature provides high-precision constraints, it is limited to separation between the two wide source categories (fossil vs biomass).[10,19] Further observational attribution to various sub-source classes requires additional source markers, such as $\delta^{13}C$.

Overall, BC is highly recalcitrant to chemical or physical transformations in the atmosphere; thus, its $\delta^{13}C$ is not appreciably affected by atmospheric processing and therefore preserves the signature of emission sources and is useful for BC source fingerprinting[20−22] (see also Supporting Information Note S3). During SAPOEX-16, the $\delta^{13}C$ signatures at MCOH and BCOB show contrasting features: BC at MCOH ($\delta^{13}C = -25.4 \pm 0.2‰$) was found to be more isotopically enriched in ^{13}C compared to BC at BCOB ($\delta^{13}C = -27.6 \pm 0.2‰$) (Figure 2). This indicates that, although the $\Delta^{14}C$ signatures are similar, the actual source composition of BC sampled at the two stations is different, suggesting differences in the relative contribution of either coal ($-23.4 \pm 1.3‰$) versus liquid fossil ($-25.5 \pm 1.3‰$) sources and/or of different biomass sources with also inherently different isotope signatures, such as C_3-plants ($-27.1 \pm 2‰$) and C_4-plants ($-13.1 \pm 1.2‰$) (see Supporting Information Note S3 and Table S5). Previous isotopic investigations of BC from South Asia were unable to differentiate any such regional differences in potential source class contributions.[13,18,19,31]

Statistical Source Estimation Using the Dual-Carbon Isotope Signals of BC. The geometry of the $\delta^{13}C$ signatures of BC at MCOH ($-25.4 \pm 0.2‰$) and BCOB ($-27.6 \pm 0.2‰$) is such that they overlap with the endmembers of three sources (C_3-biomass, coal, and liquid fossil; see Supporting Information Table S5). However, by combining the dual-C isotopes, further division of biomass and fossil sources into broader source classes can be achieved.[16,17,20−22] A complication for this − and in principle any mass balance-based source apportionment set-up − is the varying, and sometimes partially overlapping endmember ranges (e.g., $\delta^{13}C$ of liquid fossil fuel is $-25.5 \pm 1.3‰$ and coal is $-23.4 \pm 1.3‰$). To account for these effects and to quantify the associated uncertainties, a MCMC-driven Bayesian statistical approach[17] is used, which allows combining $\Delta^{14}C$ and $\delta^{13}C$ signatures as well as accounts for the variabilities, for a robust quantitative apportionment of several source classes[16,20−22] (see Methods and further details in Supporting Information Note S5; see also Supporting Information Figure S5).

While four isotope-separable source classes are here identified, which can contribute to the overall $\delta^{13}C$-BC signatures in South Asia (see Methods), separating four source

https://dx.doi.org/10.1021/acs.est.0c02193
Environ. Sci. Technol. 2020, 54, 11771−11779

classes with two source markers yields an under-determined system (see eq 2 in Supporting Information Note S5). Nonetheless, within this Bayesian approach, the probability density functions for the relative source contribution can in principle be calculated for any number of sources (see Supporting Information Figure S5), and the four-source system may thus be solved, offering perhaps the least biased analysis as the a priori information is minimal. The drawback is that it might not be possible to segregate certain source combinations; the interpretation becomes less clear. Instead, existing knowledge from the region can be used to argue why certain source combinations should be more likely. A key question in the present context is why the $\delta^{13}C$ signature of BC at MCOH is more enriched compared to that at BCOB? Both C_4-plants and fossil coal are sources with relatively more enriched $\delta^{13}C$ (see Figure 2) and may therefore offer different explanations. Thus, we explore three different scenarios, where we vary the potential impact of these two source classes.

Scenario MCMC$_4$: C$_3$, C$_4$, Liquid Fossil, and Coal. The under-determined MCMC$_4$ scenario (Supporting Information Figures S5 and S6) yields that C_3-plants is the dominating biomass source (~48%) at both sites. For BCOB, the other main source is liquid fossil (45 ± 5%), while C_4-plants and fossil coal are comparably small (7% in total). Thus, for this scenario—even within an under-determined system—we can conclude that these ^{13}C-enriched sources both have limited contributions at this site. For MCOH, the situation is more complex, since the observed isotope values are in the middle of the 'source quadrant' (Figure 2). Here, the under-determined system is challenged in differentiating between the four source classes simply because of the geometry of the observational data relative to the endmember data.

Scenario MCMC$_{3,coal}$: C$_3$, Liquid Fossil, and Coal. The MCMC$_{3,coal}$ scenario gives rather similar results (Figure 3) as the under-determined counterpart scenario MCMC$_4$ for both BCOB and MCOH. By isotopic mass conservation, both C_3-plants and coal become slightly larger and the uncertainties are reduced. However, the low coal-BC contribution at BCOB, here constrained by isotopes, is in contrast to some studies suggesting an expected high contribution from coal-BC to the BC aerosol regime in the IGP because of several thermal power plants in the region (over 70% of which are coal-fired).[32,33] Furthermore, BC concentrations reaching as high as 200 $\mu g\ m^{-3}$ have been reported in transit regions in the vicinity of such thermal power plants.[34] In fact, the coupling between the BC concentrations and air mass origin, visualized using CWT maps (Supporting Information Figure S3.c), shows that BC at BCOB (although an order lower than expected in the vicinity of power plants; Supporting Information Figure S4) mostly arrived from the IGP.

A mechanistic reason for the, perhaps unexpectedly, low coal contributions at BCOB may be that the thermally driven plume from tall smokestacks of coal-fired power plants cause the coal-BC particles to be ejected above the shallow planetary boundary layer (PBL) over the IGP during winter[35](details in Supporting Information Figures S7 and S8). Another reason may be that BC emission factors from industrial coal power plants (0.03 ± 0.03 g kg^{-1})[12] are much lower than for residential coal combustion (1.64 ± 1.73 g kg^{-1}),[12] as power plants have high combustion efficiency and widely use aerosol removal facilities.[16] For South Asia, residential usage of coal is small (<1% in total BC emissions), especially in the IGP, where biofuels such as dung cake is a more common and affordable alternative.[12,14] The low coal-BC contribution observed at BCOB may then reflect this combination of region-specific emissions and dynamics of the wintertime meteorology.

The BC lofted higher in the atmosphere from the thermal plume of power plant stacks in the continent may offer an explanation why the coal contribution at MCOH (36%) is higher relative to that at BCOB (9%) in the MCMC$_{3,coal}$ scenario. It is possible that the coal-BC, en-route to the N. Indian Ocean station, may again enter the PBL because of subsidence over the S Bay of Bengal region,[36] causing an increase in the coal-BC fraction in the aerosols. This hypothesis is supported by higher SO_4^{2-}/BC ratios over the S Bay of Bengal,[27] than in the IGP.[37] However, any addition of ^{14}C dead-C (coal-derived BC) to air masses reaching MCOH should then significantly lower the $\Delta^{14}C$-signature of BC relative to that at BCOB, unless there is also significant addition of modern-C (e.g., from large-scale biomass burning from central and southern India). The fact that the biomass-BC fraction remained similar between these stations implies that this 27% increase in coal-BC fraction at MCOH, relative to BCOB, in the MCMC$_{3,coal}$ scenario is not likely.

A potential shift of such magnitude in fossil fuel source class contributions is also at odds with any of the spatially resolved regional EIs;[12] it is thus unlikely that the source mixture of fossil-BC at MCOH would become very different during long-range transport from the main IGP source region. Taken together, the MCMC$_{3,coal}$ scenario seems viable for the isotopic fingerprint at BCOB, yet − based on a priori system knowledge − it is less likely to provide an explanation for the dual carbon isotope signatures at MCOH, which will be further addressed next.

Scenario MCMC$_{3,C4}$: C$_3$, C$_4$, and Liquid Fossil. For BCOB, this scenario − like the MCMC$_{3,coal}$ scenario − is quite similar to the MCMC$_4$ scenario; C_3-plants and liquid fossil are still the main sources (Figure 3). However, the uncertainties for this deterministic system are further reduced relative to MCMC$_4$ (from 5 to 1%). In contrast, for MCOH, the shift is larger, with the liquid fossil contribution significantly increased. The MCMC$_{3,C4}$ scenario at MCOH is quite similar to all the three different MCMC scenarios at BCOB with respect to the C_3-plants and liquid fossil contributions. The C_4-plants thus offer a perturbation that potentially explains the observed $\delta^{13}C$ enrichment at MCOH relative to BCOB.

The main source of C_4-plants in India is sugarcane.[38] January to March is the main sugarcane harvest period in PI (i.e., ~ south of 23.4°N), including subsequent agricultural crop-residue burning, while the sugarcane harvest periods are different in the northern parts.[38,39] Satellite data showed a higher density of active fire counts in PI as the winter progressed, which suggests more open burning activities in the region (Supporting Information Figure S9). This is also reflected in the contribution of GFED-derived BC-Fire (i.e., from open biomass burning) to the FEG modeled BC concentrations at MCOH (Supporting Information Table S6). The BC-Fire fraction gradually increased from 2 ± 2% (Jan) to 10 ± 5% (Feb) and finally to 17 ± 7% (Mar), which suggests that sugarcane crop residue burning in PI likely occurred during the latter half of the winter of 2016 (Feb-Mar; see further details in Supporting Information Figure S10 and Table S4). Another source of C_4-BC is from sugar mills that use bagasse (fibrous residue of sugarcane) as fuel.[12,40] These sugar mills operate for a longer period of the year in PI than in

https://dx.doi.org/10.1021/acs.est.0c02193
Environ. Sci. Technol. 2020, 54, 11771−11779

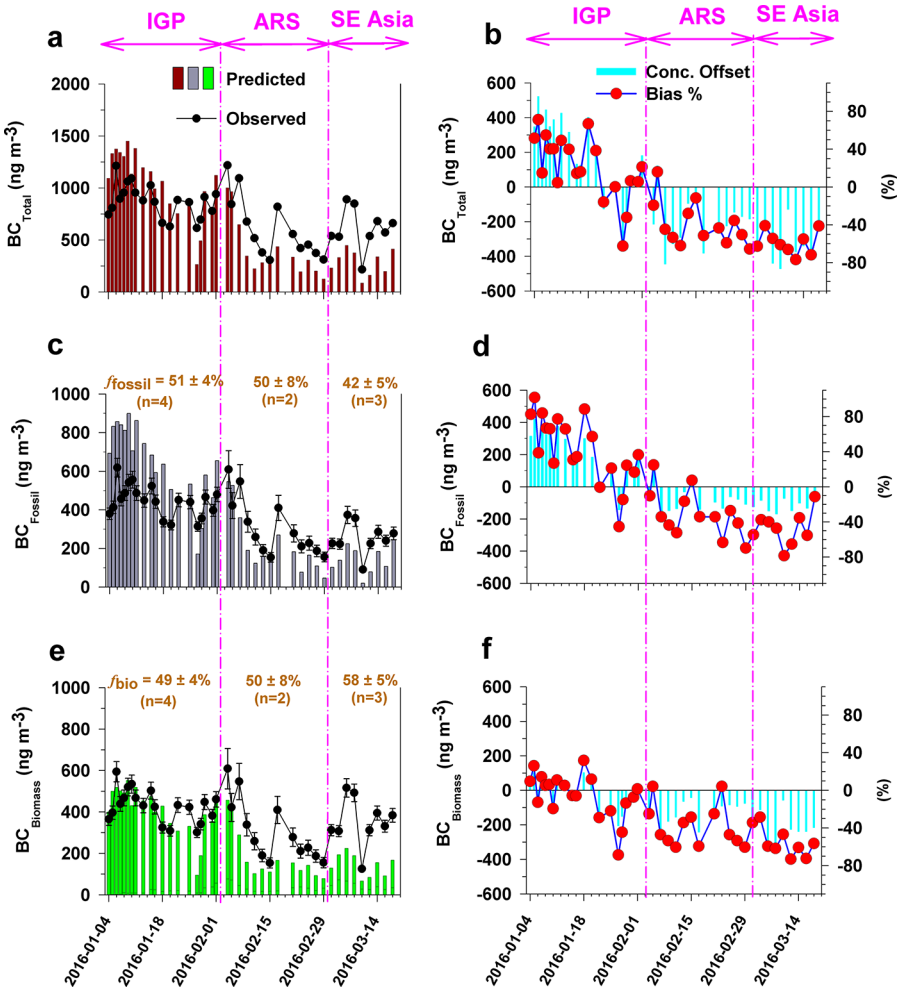

Figure 4. Panels (a), (c), and (e), respectively, show total BC concentrations, fossil, and biomass BC concentrations for observations (circles) and FEG model simulations (bars), at MCOH, respectively. Panels (b), (d), and (f) depict the concentration offsets (bars) and bias (red circles) from the corresponding model-observation comparisons. The different source regions (IGP, ARS, and SE Asia) influencing sampling at MCOH during SAPOEX-16 are identified using air mass back trajectory analysis (Supporting Information Figures S2 and S3; see also Supporting Information Note S7), and source concentrations are deconvoluted based on combination of total BC concentrations with average $\Delta^{14}C$-f_{bio} in different air mass regimes (Supporting Information Table S4).

the IGP.[39,40] Sugar mills—point sources of C_4-BC— using such low-grade fuels with commonly outdated and inefficient systems have been reported to have the highest BC emission factors (0.95 ± 0.27 g kg^{-1})[12] in the whole industry sector. The winter period (Jan to Mar) also corresponds to the period of highest production from sugar mills,[39,40] i.e., more bagasse-based C_4-BC. It is thus likely that air masses passing over PI en-route to the northern Indian Ocean and MCOH during winter (and more so between Feb-March period of SAPOEX-16; see Supporting Information Figures S2, S3, and S11) were influenced by C_4-biomass emissions, while less so for IGP during the same period where mostly paddy- and wheat crop-residue (i.e., C_3-biomass) burning is a common practice.[31,38] In conclusion, we find that the MCMC source scenarios that are most likely for BCOB and MCOH are different. For BCOB, the three different scenarios give quite similar results, but since C_4-plant burning is not prevailing in IGP during winter, while coal combustion is a continuous source, the $MCMC_{3,coal}$ best describes the relative source signatures at BCOB. The situation for MCOH is slightly different as it is highly influenced by both the IGP outflow and the air masses passing over PI on its way to the N. Indian Ocean. PI is known to have significant emissions from C_4-plants during this period,[38−40] while the coal combustion sources are smaller compared to the IGP.[12,32−34] We therefore judge the $MCMC_{3,C4}$ scenario to be the most fitting for MCOH, also since this implies a smaller change in the biomass source class contributions (up to 10% increase of C_4-biomass) relative to BCOB, compared to the massive change in fossil fuel source class contributions (up to 27% increase in coal; $MCMC_{3,coal}$) needed to be consistent with the isotope data. This conclusion is further corroborated by the FEG simulations, which suggest that the main potential geographical emission regions for MCOH during the winter period were a combination of PI and the IGP (Supporting Information Figure S11).

Model versus Observation Comparison. There has so far been limited model-observation comparison studies in South Asia,[8,9,41−43] and none for source-differentiated BC. For SAPOEX-16, the FEG model set-up produced simulations that captured the overall observed BC concentrations when averaged for the whole wintertime MCOH period (R^2 = 0.62; P <0.05; Supporting Information Figure S12). The model-predicted average BC concentration for the whole period of 700 ± 440 ng m^{-3} (SD) matched the observational

https://dx.doi.org/10.1021/acs.est.0c02193
Environ. Sci. Technol. 2020, 54, 11771−11779

average of 740 ± 250 ng m^{-3} (SD) (Figure 4a). However, temporally varying systematic offsets in BC concentrations were found in the FEG model predictions relative to observations (Figure 4b). The averaged bias (= $[BC_{model} - BC_{observed}]/BC_{model}$) for the entire period was 37 ± 20%. An overall overprediction in modeled BC for the month of January (offset: +170 ± 240 ng m^{-3}; bias: +19%) was followed by an increased underprediction in February (offset: −170 ± 150 ng m^{-3}; bias: −31%) and March (offset: −320 ± 110 ng m^{-3}; bias: −53%).

By using the average $\Delta^{14}C$-f_{bio} of samples analyzed for isotopic analysis in respective air mass clusters (IGP: n = 4; ARS: n = 2; SE Asia: n = 3), the total BC concentrations were apportioned to the corresponding concentrations deconvoluted to fossil and biomass sources at MCOH (BC_{Fossil} and $BC_{Biomass}$, respectively; see Figure 4). Comparisons with similar source-segregated FEG estimates show clear temporal trends in BC_{Fossil} and $BC_{Biomass}$, respectively (Figure 4c−f; see also Supporting Information Table S6). In January, the model-predicted average BC_{Fossil} concentrations [650 ± 200 ng m^{-3} (SD)] are somewhat higher than observations [450 ± 80 ng m^{-3} (SD)] (Figure 4c), with a monthly average bias of +50% (Figure 4d). In contrast, the model-predicted average $BC_{Biomass}$ [400 ± 120 ng m^{-3} (SD)] in January was in close agreement with the observations [430 ± 80 ng m^{-3} (SD)] (Figure 4e), with a monthly average bias of +18% (Figure 4f). The model predictions thus tend to be biased highly towards the fossil emissions in the period least affected by open-burning in South Asia and when the air masses are from the IGP region (see Supporting Information Figures S9−S11, and S13). During February to March, a simultaneous underestimation is seen in both BC_{Fossil} and $BC_{Biomass}$ predictions from the FEG model. The root-mean-square deviation (RMSD; a parameter for evaluating model-observation mismatch)[42] monotonically increased for $BC_{Biomass}$ (Jan: 0.09; Feb: 0.18; Mar: 0.22). In contrast, the RMSD became lower for BC_{Fossil} (Jan: 0.25; Feb: 0.19; Mar: 0.12), implying that the model predictions became increasingly less reliable for BC produced from biomass burning in South Asia as the winter progressed.

Deconvolution of the Model-Observation Mismatch. Model-based uncertainties can be attributed to either transport components such as the parameterization of boundary layer dynamics, aerosol processes (e.g., dry/wet deposition), or inaccuracies in EIs.[8−12,22,41−43] Given that a year-round simulation of BC concentrations with the FEG model has shown that the model parameterization well accounted for the changes in seasonal meteorology in South Asia,[42] we assume the transport modeling to be reasonably accurate even for the winter period of 2016; the discrepancies between predictions and observations then likely stem from (i) underestimation of open fires in the GFED inventory or (ii) incomplete anthropogenic emission estimates in EI-ECLIPSE.

The model-predicted overall biomass fraction at MCOH averaged 36 ± 2% without and 44 ± 8% with the inclusion of open fires, respectively; both were compared to the observed value of 52 ± 6% (Supporting Information Table S4). This contrasts to a similar comparison between the model and observations made for the European Arctic region, where including open fires (from the GFED inventory) drastically improved overall model estimates of BC concentrations.[22] Thus, for South Asia, either the fire emissions or the anthropogenic biomass emissions in EIs are underestimated. In general, increased cloudiness and potentially weak thermal signatures of small-scale burning could affect the satellite retrievals in the GFED inventory,[26,44] thereby leading to an underestimation of open fire emissions. In addition, the set of seasonally constant emission factors in GFED, representing the mean of measurements mostly for flaming combustion, to convert dry matter (burnt area) to BC may not be uniform worldwide and thereby could present a large regional variability.[26,44] Nonetheless, the explanation for the overall model-observation mismatch in sources is not just a miscalculation of BC from open fire contribution alone; it is likely also because of issues in the regional emission distribution in the global EI-ECLIPSE.

Systematic offsets with regard to BC emission fluxes in an incomplete EI are a plausible explanation. This is supported by the observation that the 2010 scenario of EI-ECLIPSE estimated the major contribution of BC to originate from the IGP in N. India and in a few pockets of W. India.[25,42] In contrast, peninsular Indian BC emissions, preferentially reaching MCOH (Supporting Information Figure S13), were predicted to be relatively low. This agrees with the finding that the bias in simulated BC versus observed BC concentrations was indeed the highest during periods of transport from the peninsular Indian region (mostly between Feb and Mar; see Figure 4f and Supporting Information Figure S13), further supporting the notion that the systematic underestimation of anthropogenic biomass emission from the peninsular Indian region of EI-ECLIPSE is the likely cause for the wintertime model-observation bias in South Asia.

Taken together, this study shows that the characteristics for BC sources in the IGP outflow are similar to those intercepted in the N. Indian Ocean. The main difference is a small yet significant contribution (up to 10%) from peninsular Indian C_4 biomass-BC emissions (from sugarcane crop residue burning) to the wider wintertime S Asian continental outflow. Furthermore, we find that model simulations agree (within a factor of 2) with observations of BC concentrations, yet there is a systematic time-dependent bias (+19 to −53%); identifying aspects for improvement in the BC EIs and highlighting also the importance of these for correct time-resolved model predictions. Overall, biomass and fossil combustion sources contribute equally to BC during winter and the contributions are regionally homogenous across South Asia.[13,18,19,31] The fossil-BC emissions are overestimated in the IGP region, while biomass-BC emissions are underestimated in PI in EIs leading to the model-observation mismatch for South Asia. These findings pinpoint opportunities for improving emission estimates in EIs and directing policy efforts for mitigation of BC climate and air pollution impact in one of the most polluted regions in the world, South Asia.

■ ASSOCIATED CONTENT

Supporting Information

The Supporting Information is available free of charge at https://pubs.acs.org/doi/10.1021/acs.est.0c02193.

Discussions on the South Asia-specific radiocarbon biomass endmember and fractionation effects in biomass source classes; methodological details of Bayesian modeling, FEG modeling, and air mass back trajectory analysis; back trajectories analysis, BC concentrations, Bayesian modeling scenarios and results, satellite-derived fire counts, and GFED based BC_{Fire}, model-based

https://dx.doi.org/10.1021/acs.est.0c02193
Environ. Sci. Technol. 2020, 54, 11771−11779

footprint emission sensitivities and source contributions; sampling details and isotope and FEG data (PDF)

AUTHOR INFORMATION

Corresponding Author

Örjan Gustafsson − *Department of Environmental Science, and the Bolin Centre for Climate Research, Stockholm University, Stockholm 10691, Sweden*; Phone: +46 70 324 73 17; Email: orjan.gustafsson@aces.su.se

Authors

Sanjeev Dasari − *Department of Environmental Science, and the Bolin Centre for Climate Research, Stockholm University, Stockholm 10691, Sweden*; orcid.org/0000-0001-7222-7982

August Andersson − *Department of Environmental Science, and the Bolin Centre for Climate Research, Stockholm University, Stockholm 10691, Sweden*; orcid.org/0000-0002-4659-7055

Andreas Stohl − *Norwegian Institute for Air Research (NILU), Kjeller 2027, Norway*

Nikolaos Evangeliou − *Norwegian Institute for Air Research (NILU), Kjeller 2027, Norway*; orcid.org/0000-0001-7196-1018

Srinivas Bikkina − *Department of Environmental Science, and the Bolin Centre for Climate Research, Stockholm University, Stockholm 10691, Sweden*; orcid.org/0000-0001-8519-012X

Henry Holmstrand − *Department of Environmental Science, and the Bolin Centre for Climate Research, Stockholm University, Stockholm 10691, Sweden*

Krishnakant Budhavant − *Department of Environmental Science, and the Bolin Centre for Climate Research, Stockholm University, Stockholm 10691, Sweden; Maldives Climate Observatory at Hanimaadhoo (MCOH), Maldives Meteorological Services, Hanimaadhoo 02020, Republic of the Maldives; Divecha Centre for Climate Change, Indian Institute of Science, Bangalore 560012, India*; orcid.org/0000-0003-2753-3192

Abdus Salam − *Department of Chemistry, University of Dhaka, Dhaka 1000, Bangladesh*

Complete contact information is available at: https://pubs.acs.org/10.1021/acs.est.0c02193

Author Contributions

Ö.G. and A.A. designed the observation-based source apportionment and together with A.S. and N.E. performed the observation-model comparison. Samples were collected by S.D., S.B., H.H., and K.B. at MCOH and by Ab.S. at BCOB. A.A. was in charge of the MCMC simulation while A.S. and N.E. were in charge of model simulations. S.D. analyzed the samples. S.D., Ö.G., and A.A. interpreted the data, wrote the paper, and produced the figures, with input from all co-authors. All authors have given approval to the final version of the manuscript.

Funding

This work was supported by research grants from the Swedish Research Council for Sustainable Development (FORMAS contract no. 942−2015-1061) and the Swedish Research Council (VR contract no. 2015−03279; 2017−01601).

Notes

The authors declare no competing financial interest.

ACKNOWLEDGMENTS

We thank the technicians at BCOB and MCOH for their support with field operations. The authors specially thank the Maldives Meteorological Services (MMS), the government of the Republic of the Maldives, and the University of Dhaka for continued support towards the joint operation of MCOH and BCOB, respectively. This study also benefited from the research environment provided by the Bolin Centre for Climate Research at Stockholm University.

REFERENCES

(1) Ramanathan, V.; Carmicheal, G. Global and regional climate changes due to black carbon. *Nat. Geosci.* **2008**, *1*, 221−227.

(2) Bond, T. C.; Doherty, S. J.; Fahey, D. W.; Forster, P. M.; Berntsen, T.; DeAngelo, B. J.; Flanner, M. G.; Ghan, S.; Kärcher, B.; Koch, D.; Kinne, S.; Kondo, Y.; Quinn, P. K.; Sarofim, M. C.; Schultz, M. G.; Schulz, M.; Venkataraman, C.; Zhang, H.; Zhang, S.; Bellouin, N.; Guttikunda, S. K.; Hopke, P. K.; Jacobson, M. Z.; Kaiser, J. W.; Klimont, Z.; Lohmann, U.; Schwarz, J. P.; Shindell, D.; Storelvmo, T.; Warren, S. G.; Zender, C. S. Bounding the role of black carbon in the climate system: a scientific assessment. *J. Geophys. Res.* **2013**, *118*, 5380−5552.

(3) *Climate change 2013*: *The physical basis*; https://www.ipcc.ch/report/ar5/wg1/, 2013.

(4) Menon, S.; Koch, D.; EIg, G.; Sahu, S.; Fasullo, J.; Orlikowski, D. Black carbon aerosols and the third polar ice cap. *Atmos. Chem. Phys.* **2010**, *10*, 4559−4571.

(5) Burney, J.; Ramanathan, V. Recent climate and air pollution impacts on Indian agriculture. *Proc. Natl. Acad. Sci. U. S. A.* **2014**, *111*, 16319−16324.

(6) Health effects of black carbon; http://www.euro.who.int/__data/assets/pdf_file/0004/162535/e96541.pdf, 2012.

(7) Gustafsson, Ö.; Ramanathan, V. Convergence on climate warming by black carbon aerosols. *Proc. Natl. Acad. Sci. U. S. A.* **2016**, *113*, 4243−4245.

(8) Kumar, R.; Barth, M. C.; Nair, V. S.; Pfister, G. G.; Suresh Babu, S.; Satheesh, S. K.; Krishna Moorthy, K.; Carmichael, G. R.; Lu, Z.; Streets, D. G. Sources of black carbon aerosols in South Asia and surrounding regions during the Integrated Campaign for Aerosols, Gases and Radiation Budget (ICARB). *Atmos. Chem. Phys.* **2015**, *15*, 5415−5428.

(9) Kumar, R.; Barth, M. C.; Pfister, G. G.; Nair, V. S.; Ghude, S. D.; Ojha, N. What controls the seasonal cycle of black carbon aerosols in India? *J. Geophys. Res. Atmos.* **2015**, *120*, 7788−7812.

(10) Chen, B.; Andersson, A.; Lee, M.; Kirilova, E. N.; Xiao, Q.; Kruså, M.; Shi, M.; Hu, K.; Lu, Z.; Streets, D. G.; Du, K.; Gustafsson, Ö. Source forensics of black carbon aerosols from China. *Environ. Sci. Technol.* **2013**, *47*, 9102−9108.

(11) Zhao, Y.; Nielsen, C. P.; Lei, Y.; McElroy, M. B.; Hao, J. Quantifying the uncertainties of a bottom-up emission inventory of anthropogenic atmospheric pollutants in China. *Atmos. Chem. Phys.* **2011**, *11*, 2295−2308.

(12) Paliwal, U.; Sharma, M.; Burkhart, J. F. Monthly and spatially resolved black carbon emission inventory of India: uncertainty analysis. *Atmos. Chem. Phys.* **2016**, *16*, 12457−12476.

(13) Gustafsson, Ö.; Kruså, M.; Zencak, Z.; Sheesley, R. J.; Granat, L.; Engström, E.; Praveen, P. S.; Rao, P. S. P.; Leck, C.; Rodhe, H. Brown clouds over South Asia: biomass or fossil fuel combustion? *Science* **2009**, *323*, 495−498.

(14) Venkataraman, C.; Habib, G.; Eiguren-Fernandez, A.; Miguel, A. H.; Friedlander, S. K. Residential biofuels in South Asia: carbonaceous aerosol emissions and climate impacts. *Science* **2005**, *307*, 1454−1456.

(15) Fuzzi, S.; Baltensperger, U.; Carslaw, K.; Decesari, S.; Denier van der Gon, H.; Facchini, M. C.; Fowler, D.; Koren, I.; Langford, B.; Lohmann, U.; Nemitz, E.; Pandis, S.; Riipinen, I.; Rudich, Y.; Schaap, M.; Slowik, J.; Spracklen, D. V.; Vignati, E.; Wild, M.; Williams, M.;

Gilardoni, S. Particulate matter, air quality and climate: lessons learned and future needs. *Atmos. Chem. Phys.* **2015**, *15*, 8217−8299.
(16) Ni, H.; Huang, R. J.; Cao, J.; Liu, W.; Zhang, T.; Wang, M.; Meijer, H. A. J.; Dusek, U. Source apportionment of carbonaceous aerosols in Xi'an, China: insights from a full year of measurements of radiocarbon and the stable isotope ^{13}C. *Atmos. Chem. Phys.* **2018**, *18*, 16363−16383.
(17) Andersson, A.; Deng, J.; Ke, D.; Zheng, M.; Yan, C.; Sköld, M.; Gustafsson, Ö. Regionally-varying combustion sources of the January 2013 severe haze events over eastern China. *Environ. Sci. Technol.* **2015**, *49*, 2038−2043.
(18) Bosch, C.; Andersson, A.; Kirillova, E. N.; Budhavant, K.; Tiwari, S.; Praveen, P. S.; Russell, L. M.; Beres, N. D.; Ramanathan, V.; Gustafsson, Ö. Source-diagnostic dual-isotope composition and optical properties of water-soluble organic carbon and elemental carbon in the South Asian outflow intercepted over the Indian Ocean. *J. Geophys. Res. Atmos.* **2014**, *119*, 11743−11,759.
(19) Budhavant, K.; Andersson, A.; Bosch, C.; Kruså, M.; Kirillova, E. N.; Sheesley, R. J.; Safai, P. D.; Rao, P. S. P.; Gustafsson, Ö. Radiocarbon-based source apportionment of elemental carbon aerosols at two South Asian receptor observatories over a full annual cycle. *Environ. Res. Lett.* **2015**, *10*, No. 064004.
(20) Fang, W.; Du, K.; Andersson, A.; Xing, Z.; Cho, C.; Kim, S. W.; Deng, J.; Gustafsson, Ö. Dual-isotope constraints on seasonally resolved source fingerprinting of black carbon aerosols in sites of the four emission hot spot regions of China. *J. Geophy. Res. Atmos.* **2018**, *123*, 11,735−11,747.
(21) Li, C.; Bosch, C.; Kang, S.; Andersson, A.; Chen, P.; Zhang, Q.; Cong, Z.; Chen, B.; Qin, D.; Gustafsson, Ö. Sources of black carbon to the Himalayan−Tibetan Plateau glaciers. *Nat. Comm.* **2016**, *7*, 12574.
(22) Winiger, P.; Andersson, A.; Eckhardt, S.; Stohl, A.; Gustafsson, Ö. The sources of atmospheric black carbon at a European gateway to the Arctic. *Nat. Comm.* **2016**, *7*, 12776.
(23) Stohl, A.; Hittenberger, M.; Wotawa, G. Validation of the lagrangian particle dispersion model FLEXPART against large-scale tracer experiment data. *Atmos. Environ.* **1998**, *32*, 4245−4264.
(24) Stohl, A.; Forster, C.; Frank, A.; Seibert, P.; Wotawa, G. Technical note: the Lagrangian particle dispersion model FLEXPART version 6.2. *Atmos. Chem. Phys.* **2005**, *5*, 2461−2474.
(25) Stohl, A.; Aamaas, B.; Amann, M.; Baker, L. H.; Bellouin, N.; Berntsen, T. K.; Boucher, O.; Cherian, R.; Collins, W.; Daskalakis, N.; Dusinska, M.; Eckhardt, S.; Fuglestvedt, J. S.; Harju, M.; Heyes, C.; Hodnebrog, Ø.; Hao, J.; Im, U.; Kanakidou, M.; Klimont, Z.; Kupiainen, K.; Law, K. S.; Lund, M. T.; Maas, R.; MacIntosh, C. R.; Myhre, G.; Myriokefalitakis, S.; Olivié, D.; Quaas, J.; Quennehen, B.; Raut, J. C.; Rumbold, S. T.; Samset, B. H.; Schulz, M.; Seland, Ø.; Shine, K. P.; Skeie, R. B.; Wang, S.; Yttri, K. E.; Zhu, T. Evaluating the climate and air quality impacts of short-lived pollutants. *Atmos. Chem. Phys.* **2015**, *15*, 10529−10566.
(26) van der Werf, G. R.; Randerson, J. T.; Giglio, L.; van Leeuwen, T. T.; Chen, Y.; Rogers, B. M.; Mu, M.; van Marle, M. J. E.; Morton, D. C.; Collatz, G. J.; Yokelson, R. J.; Kasibhatla, P. S. Global fire emissions estimates during 1997−2016. *Earth Syst. Sci Data* **2017**, *9*, 697−720.
(27) Dasari, S.; Andersson, A.; Bikkina, S.; Holmstrand, H.; Budhavant, K.; Satheesh, S.; Asmi, E.; Kesti, J.; Backman, J.; Salam, A.; Bisht, D. S.; Tiwari, S.; Hameed, Z.; Gustafsson, Ö. Photochemical degradation affects the light absorption of water-soluble brown carbon in the South Asian outflow. *Sci. Adv.* **2019**, *5*, eaau8066.
(28) Muhammad, T.; Przemyslaw, J. Electric energy access in Bangladesh. *Trans. Environ.Elect. Eng.* **2016**, *1*, 6−17.
(29) Turnbull, J. C.; Fletcher, S. E. M.; Ansell, I.; Brailsford, G. W.; Moss, R. C.; Norris, M. W.; Steinkamp, K. Sixty years of radiocarbon dioxide measurements at Wellington, New Zealand: 1954−2014. *Atmos. Chem. Phys.* **2017**, *17*, 14771−14784.
(30) Andersson, A. A systematic examination of a random sampling strategy for source apportionment calculations. *Sci. Tot. Environ.* **2011**, *412-413*, 232−238.
(31) Bikkina, S.; Andersson, A.; Kirillova, E. N.; Holmstrand, H.; Tiwari, S.; Srivastava, A. K.; Bisht, D. S.; Gustafsson, Ö. Air quality in megacity Delhi affected by countryside biomass burning. *Nat.Sustain.* **2019**, *2*, 200−205.
(32) Gogoi, M. M.; Jayachandran, V. N.; Vaishya, A.; Babu, S. N. S.; Satheesh, S. K.; Moorthy, K. K. Airborne in situ measurements of aerosol size distributions and black carbon across the Indo-Gangetic Plain during SWAAMI−RAWEX. *Atmos. Chem. Phys.* **2020**, *20*, 8593−8610.
(33) Sahu, S. K.; EIg, G.; Sharma, C. Decadal growth of black carbon emissions in India. *Geophys. Res. Lett.* **2008**, *35*, L02807.
(34) Singh, R. P.; Kumar, S.; Singh, A. K. Elevated Black Carbon Concentrations and Atmospheric Pollution around Singrauli Coal-Fired Thermal Power Plants (India) Using Ground and Satellite Data. *Int J Environ Res Public Health.* **2018**, *15*, 2472.
(35) Nair, V. S.; Moorthy, K. K.; Alappattu, D. P.; Kunhikrishnan, P. K.; George, S.; Nair, P. R.; Babu, S. S.; Abish, B.; Satheesh, S. K.; Tripathi, S. N.; Niranjan, K.; Madhavan, B. L.; Srikant, V.; Dutt, C. B. S.; Badarinath, K. V. S.; Reddy, R. R. Wintertime aerosol characteristics over the Indo-Gangetic Plain (IGP): Impacts of boundary layer processes and long-range transport. *J. Geophys. Res.* **2007**, *112*, D13025.
(36) Lawrence, M. G.; Lelieveld, J. Atmospheric pollutant outflow from southern Asia: A review. *Atmos. Chem. Phys.* **2010**, *10*, 11017−11096.
(37) Bikkina, S.; Sarin, M. M. $PM_{2.5}$, EC and OC in atmospheric outflow from the Indo-Gangetic Plain: Temporal variability and aerosol organic carbon-to-organic mass conversion factor. *Sci. Tot. Environ.* **2014**, *487*, 196.
(38) Jain, N.; Bhatia, A.; Pathak, H. Emission of air pollutants from crop residue burning in India. *Aerosol Air Qual. Res.* **2014**, *14*, 422−430.
(39) The Indian Sugar Industry Sector Roadmap- KPMG India; http://www.in.kpmg.com/pdf/indian_sugar_industry.pdf, 2017.
(40) Sahu, S. S.; Ohara, T. T.; EIg, G. G.; Kurokawa, J. J.; Nagashima, T. T. Rising critical emission of air pollutants from renewable biomass based cogeneration from the sugar industry in India. *Environ. Res. Lett.* **2015**, *10*, No. 095002.
(41) Moorthy, K. K.; Beeguma, S. N.; Srivastava, N.; Satheesh, S. K.; Chin, M.; Blond, N.; Babu, S. S.; Singh, S. Performance evaluation of chemistry transport models over India. *Atmos. Environ.* **2013**, *71*, 210−225.
(42) Gadhavi, H. S.; Renuka, K.; Ravi Kiran, V.; Jayaraman, A.; Stohl, A.; Klimont, Z.; EIg, G. Evaluation of black carbon emission inventories using a Lagrangian dispersion model − a case study over southern India. *Atmos. Chem. Phys.* **2015**, *15*, 1447−1461.
(43) Govardhan, G.; Satheesh, S. K.; Moorthy, K. K.; Nanjundiah, R. Simulations of black carbon over the Indian region: improvements and implications of diurnality in emissions. *Atmos. Chem. Phys.* **2019**, *19*, 8229−8241.
(44) van der Werf, G. R.; Randerson, J. T.; Giglio, L.; Collatz, G. J.; Kasibhatla, P. S.; Arellano, A. F., Jr. Interannual variability in global biomass burning emissions from 1997 to 2004. *Atmos. Chem. Phys.* **2006**, *6*, 3423−3441.

https://dx.doi.org/10.1021/acs.est.0c02193
Environ. Sci. Technol. 2020, 54, 11771−11779